Self-Assembly of Alkali-Soluble [60]Fullerene Containing Poly(methacrylic acid) in Aqueous Solution

Palaniswamy Ravi,[†,‡] Sheng Dai,[†,‡] Chung How Tan,[‡] and Kam Chiu Tam*[,†,‡,§]

Singapore-MIT Alliance, School of Mechanical and Production Engineering, Division of Chemical & Biomolecular Engineering, College of Engineering, Nanyang Technological University, 50 Nanyang Avenue, Singapore 639798, Republic of Singapore

Received September 21, 2004; Revised Manuscript Received November 8, 2004

ABSTRACT: Well-defined stimuli-responsive alkali-soluble poly(methacrylic acid)-*block*-[60]fullerene (PMAA-*b*-C_{60}) was synthesized via atom transfer radical polymerization (ATRP), and its aggregation behavior in aqueous solution was examined using potentiometric and conductometric titrations, static and dynamic light scattering, and transmission electron microscopic (TEM) techniques. PMAA-*b*-C_{60} shows pH-responsive and water-soluble properties at high pH. In dilute solution, the micelles and large secondary aggregates, which are independent of polymer concentration, coexist in solution. The R_h of micelles increases from 6 to 10 nm with increasing degree of neutralization and remains constant at 10 nm with the addition of salt. However, the R_h of large aggregates increases from 91 to 153 nm with increasing degree of neutralization and decreases from 153 to 105 nm with increasing NaCl concentration. TEM studies revealed that the large aggregates comprise of individual micelles and possess microstructure similar to large compound micelles (LCM).

Introduction

Self-assembly of amphiphilic block copolymers are potential systems that can be used to prepare nanoscale aggregates of different morphologies in aqueous solution. The study on the self-assembly behavior of well-defined polymeric systems such as the aggregate morphology and the aggregation mechanism in solution are of potential interest to the research community. Much interest has been focused on the self-assembled structure of polyelectrolyte containing amphiphilic block copolymers in aqueous solution, which respond to external stimuli such as pH, temperature, or ionic strength.[1,2] Hydrophobic interaction and electrostatic repulsion are the main driving forces in controlling the self-assembly behavior of polyelectrolyte containing block copolymers. In aqueous solution, the hydrophobic moieties form the micellar core, which is stabilized by ionic corona segments.[3] In addition, micellization normally occurs at very low critical micelle concentration (cmc) due to the poor compatibility between the ionic and hydrophobic segments.[4,5] By increasing the polymer concentration or altering the composition of the copolymer, different types of aggregate can be obtained.

Laser light scattering is among one the most versatile research tools for studying the self-assembled microstructure. In addition, the direct morphological investigation by transmission electron microscopy (TEM) provides images of aggregates that could further be used to confirm the microstructure determined from light scattering studies.[6−8] Eisenberg and co-workers reported the formation of star or crew-cut micelles of block copolymers, which depended on the hydrophobic−hydrophilic balance between the two blocks.[8] Various types of aggregates such as cylindrical structure, core−shell structure,[9] vesicle-like structure,[4,10] three-layer vesicular micelles,[11] onionlike multilayer micelles,[12] crew-cut micelles,[8] and large compound micelles[13] have been reported. Fusion of polyelectrolyte micelles into vesicles and fractal toroid micronetworks has been reported by increasing the polymer and salt concentration of poly(ethylethylene-*b*-styrenesulfonic acid) polymer.[10]

[60]Fullerene (C_{60}) has received extensive attention due to its unique chemical and physical properties.[14,15] However, because of its poor solubility and processability, many of its potential applications are hampered. To overcome this problem, several approaches have been adopted, such as surfactant solubilization,[16] charge-transfer complex formation through electron donator−acceptor interaction,[17] and synthesis of fullerene derivatives by conjugating small functional groups or long-chain polymers onto C_{60} molecules.[18] The extremely hydrophobic C_{60} can be solubilized in aqueous solution[19] by derivatizing C_{60} with hydrophilic functional groups such as carboxylic acids,[20,21]amines,[22,23] metal anions,[24] and alcohols.[25] In recent years, research on C_{60}-containing polymers has intensified since the unique properties of C_{60} combined with the macromolecular characteristics are retained after conjugation with polymers. These polymers are soluble in organic solvents, which not only facilitates the processability but also enhances its potential applications in various disciplines.[26,27] Blocking hydrophilic polymeric chains onto C_{60} can increase its solubility in aqueous solution.[18,28] Fullerene conjugated with well-defined polymers could also form nanoscale aggregates in organic solvents,[29] or in aqueous solutions,[30] due to their amphiphilic character. For C_{60}-containing polyelectrolytes, the chemical structure, the molecular weight, and the concentration of polymer together with the ionic strength and pH play important roles in controlling the morphology of the aggregates. Until recently, there are only a few papers describing the aggregation behavior of fullerene-containing polymers. Large spherical-like compound aggregates of C_{60} end-capped poly(ethylene oxide)s were

† Singapore-MIT Alliance.
‡ School of Mechanical and Production Engineering.
§ Division of Chemical & Biomolecular Engineering.
* Corresponding author: Fax (65) 6791-1859; e-mail mkctam@ntu.edu.sg.

10.1021/ma0480547 CCC: $30.25
Published on Web 01/07/2005

observed in polar solvents.[31] C_{60} grafted with well-defined polystyrene or poly(*p*-vinylphenol) was synthesized, and the micellization behavior in THF was examined.[32] Wang et al. studied the micellization behavior of fullerene-containing poly(alkyl methacrylate)s in THF and reported the existence of individual polymer chains along with core−shell aggregates.[33] Yang and coworkers recently published the aggregation behavior of poly(acrylic acid)-*b*-C_{60} in aqueous solution, where core−shell-like structure was observed, and the microstructure influenced the photoconductive properties.[30] Recently, we have synthesized well-defined poly(*tert*-butyl methacrylate)-*b*-C_{60} and studied its aggregation behavior in chlorobenzene/ethyl acetate solvent mixtures.[29] Most of the aggregation behavior of C_{60}-containing polymers was conducted in organic solvents, and there is a scarcity of reports on the self-assembly behaviors of well-defined pH-responsive water-soluble fullerene-containing polymers.

Synthesis of water-soluble polymeric C_{60} derivatives with well-defined structures is challenging. Only very few studies have been conducted on the blocking of well-defined polymeric architecture onto C_{60} using the living free radical polymerization technique. The blocking of well-defined monosubstituted polystyrene on C_{60} was first attempted using TEMPO by Ford et al.[34] Atom transfer radical polymerization technique (ATRP) was used for the first time to synthesize well-defined C_{60} end-capped polystyrene and polymethacrylate.[35] Yang and co-workers demonstrated the use of ATRP for the synthesis of well-defined water-soluble poly(acrylic acid)-*b*-C_{60} (PAA-*b*-C_{60}) polymer.[30] Fullerene-terminated well-defined poly(*tert*-butyl acrylate-*b*-styrene) (P(*t*BA-*b*-St) was synthesized by reacting C_{60} with azide end-capped P(*t*BA-*b*-St)) copolymer prepared by ATRP.[36] Very recently, we have synthesized well-defined water-soluble poly(2-(dimethylamino)ethyl methacrylate)-*b*-C_{60} polymer and demonstrated the aggregation behavior as a function of pH and temperature.[37] Although there are only a few reported studies on the synthesis of well-defined monosubstituted polymeric C_{60} derivatives, detailed studies on their aggregation behaviors and productions of interesting morphology in aqueous solution especially using external stimuli are scare. In this study, a well-defined poly(methacrylic acid)-*b*-C_{60} (PMAA-*b*-C_{60}) was synthesized by ATRP, and its aggregation behavior in aqueous solution were further elucidated using potentiometric and conductometric titrations, laser light scattering, and transmission electron microscopic techniques.

Experimental Section

Materials. C_{60} (>99.5%) and *tert*-butyl methacrylate (*t*BMA, 98%) monomer were purchased from MTR Ltd. and Sigma-Aldrich, respectively. 1,1,4,7,10,10-Hexamethyltriethylenetetramine (HMTETA, Aldrich 97%), CuCl (Aldrich 99.99%), and *p*-toluenesulfonyl chloride (Fluka, 99%) were used as received. *t*BMA was passed through a basic alumina column, dried over CaH_2, and distilled under reduced pressure. All the solvents used in the experiments were freshly distilled. Deionized water used was from a Millipore Alpha-Q purification system equipped with a 0.22 μm filter, while HCl, NaOH, and NaCl (Merck) were used to adjust the pH and the ionic strength of polymer solutions.

Synthesis of P*t*BMA-Cl Macroinitiator. In the first step, well-defined −Cl-terminated P*t*BMA macroinitiator was synthesized using *p*-toluenesulfonyl chloride as the initiator and CuCl complexed with HMTETA as a catalyst in 50 vol % anisole at 90 °C.[38] After 90% conversion was attained, the reaction was stopped by diluting the reaction mixture with THF, and the catalyst system was removed by passing through an alumina column. The polymer was recovered by precipitating into a large excess of water/methanol (1:1) mixture. The reprecipitation was repeated three times. The polymer was dried under vacuum at room temperature. M_n = 16 000 Da, M_w/M_n = 1.13.

Synthesis of PMAA-*b*-C_{60}. P*t*BMA-Cl macroinitiator and C_{60} (2.5 equiv to macroinitiator) were dissolved into 1,2-dichlorobenzene in a Schlenk flask. In a separate Schlenk flask, the CuCl/HMTETA catalyst system (2:2:1, CuCl:HMTETA:P*t*BMA-Cl) was dissolved in a small amount 1,2-dichlorobenzene. Three freeze−pump−thaw cycles were performed for both the Schlenk flasks to remove the traces of oxygen. Finally, under an argon atmosphere, the CuCl/HMTETA catalyst system was added via a double-tipped needle and allowed to react for 40 h at 90 °C. Then, the reaction mixture was diluted with THF, the catalyst was removed by passing through an alumina column, and the solvents (both THF and 1,2-dichlorobenzene) were completely removed by vacuum. The unreacted C_{60} was removed by dissolving the polymer in THF, and it is then filtered and passed through a neutral alumina column. The solution was concentrated and precipitated in large excess of water/methanol (1:1) mixture to yield a dark brown polymer. The procedure was repeated three times to ensure the complete removal of unreacted C_{60}. The polymer was then dried under vacuum and stored in the dark. M_n = 16 100 Da and M_w/M_n = 1.18. Subsequently, the *tert*-butyl protecting groups on the P(*t*BMA) block were hydrolyzed with concentrated hydrochloric acid in 1,4-dioxane at 85 °C for 6 h to form a PMAA block. FT-IR (KBr pellet) showed the broad peak at 3500 cm^{-1}, which is the characteristic absorption for carboxylic acid. The content of the acid was further quantified by potentiometric titration which is consistent with the GPC result.

Gel Permeation Chromatography (GPC). An Agilent 1100 series GPC system equipped with a LC pump, PLgel 5 μm MIXED-C column, and RI detector and RI/UV dual detector systems was used to determine the polymer molecular weight and molecular weight distribution. The column was calibrated with narrow molecular weight polystyrene standards. HPLC grade THF stabilized with BHT was used as a mobile phase. The flow rate was maintained at 1.0 mL/min. The wavelength of the UV detector was set to 330 nm.

Spectroscopy. An HP8453 UV−vis spectrophotometer was used to measure the absorption of the copolymer solutions. The FT-IR spectrum was recorded using a Biorad FTS 6000 spectrometer at room temperature using a KBr pellet. The ^{13}C NMR spectrum for the copolymer was measured using a Brüker DRX400 instrument in $CDCl_3$.

Thermogravimetric Analysis (TGA). A Perkin-Elmer TGA7 thermogravimetric analyzer was used to conduct the TGA measurements. The temperature was scanned from 25 to 800 °C with a scan rate of 10 °C/min under nitrogen (N_2) flow.

Potentiometric and Conductometric Titration. A Radiometer ABU93 triburet titrator equipped with Aliquot software was used to conduct the titration experiments. The temperature was controlled with a PolyScience water bath. In addition, a Metrohm 744 pH meter equipped with a Solitrode combined pH electrode was used to measure the pH values of the sample solutions for light scattering experiments.

Laser Light Scattering (LLS). A Brookhaven BI-200SM goniometer system equipped with a 522-channel BI9000AT digital multiple τ correlator was used to perform laser light scattering experiments. For static light scattering (SLS), a Berry plot was used to analyze the experimental data, and the d*n*/d*C* values were measured using a Brookhaven BI-DNDC differential refractometer. For dynamic light scattering (DLS), the inverse Laplace transform of REPES in the Gendist software package was used to analyze the time correlation functions with probability of reject setting at 0.5. A 0.45 μm filter was used to remove dust prior to the light scattering experiments, and the temperatures were controlled by a PolyScience water bath.

Scheme 1. Synthesis Scheme of PMAA-*b*-C_{60} Using the ATRP Technique

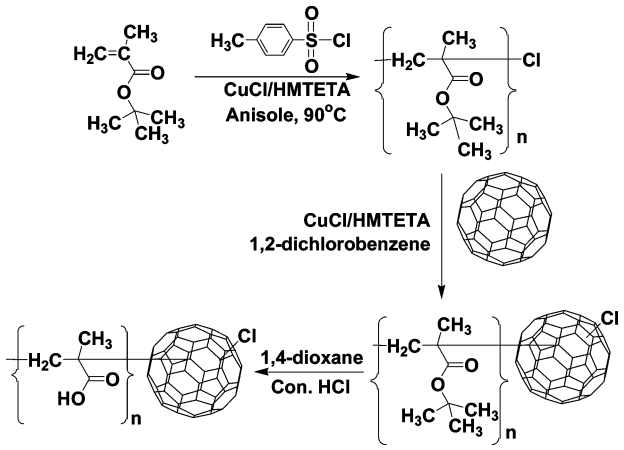

Transmission Electron Microscopy (TEM). Transmission electron microscopic studies were conducted using a JEOL JEM-2010 transmission electron microscope operating at 200 kV. Copper gird precoated with carbon was placed on a filter paper. A drop of filtered polymer solution was placed onto the copper grid and allowed to dry at atmospheric condition overnight.

Results and Discussion

PMAA-*b*-C_{60} Synthesis and Characterization. It was demonstrated recently that ATRP is a versatile technique for the synthesis of well-defined C_{60}-containing polymers.[30,35] The synthesis of PMAA-*b*-C_{60} is described in Scheme 1. First, well-defined stable −Cl-terminated P*t*BMA macroinitiator was synthesized by ATRP as described in the Experimental Section. From GPC traces, it was found that well-defined P*t*BMA-Cl was obtained with M_n = 16 000 Da and M_w/M_n = 1.13. To obtain P*t*BMA-*b*-C_{60} copolymer, ATRP was utilized again, and the details have been described in the Experimental Section. To avoid multiple substitutions of polymer chains onto C_{60}, a higher ratio of C_{60}:P*t*BMA-Cl (2.5:1) was used. The GPC traces of the P*t*BMA-*b*-C_{60} polymer measured using an RI detector showed unimodel distribution with M_n = 16 100 Da and M_w/M_n = 1.18. A comparison of the GPC traces of the P*t*BMA macroinitiator and fullerene-containing P*t*BMA using RI detector is shown in Figure 1. The small contribution of the compact C_{60} molecule to the hydrodynamic volume might be responsible for the observed small increase in the molecular weight of the fullerene-containing polymer. In addition, the absence of tailing or multiple peaks is also evident from the RI detector, confirming the monoaddition of P*t*BMA to C_{60} molecules. The covalent bonding between the C_{60} and P*t*BMA was further confirmed using UV/RI dual mode detectors. Figure 1 also compared the GPC traces of the P*t*BMA-C_{60} measured using UV/RI dual mode detectors. Since only C_{60} moiety containing polymers were detectable by the UV detector, it is evident from the figure that the P*t*BMA was covalently bonded to C_{60}. The GPC traces of P*t*BMA-*b*-C_{60} detected from both UV and RI detectors are nearly identical, indicating the chemical uniformity of the polymer. However, a slightly broader peak was observed from the UV detector compared to RI detector, which is possibly related to the absorption phenomena rather than size exclusion. It is possible that minute fractions of unreacted P*t*BMA-Cl may be present, and this small fraction is extremely difficult to remove

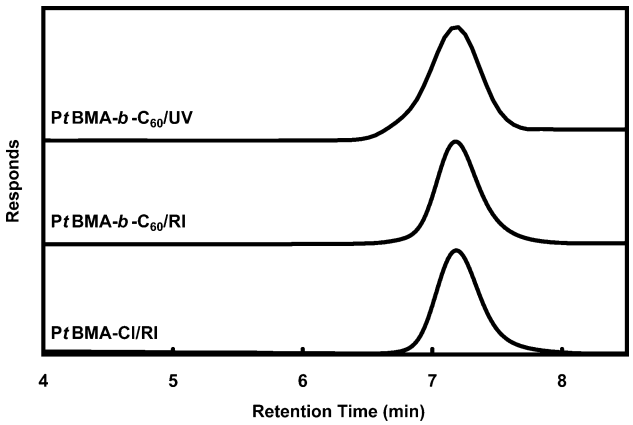

Figure 1. GPC traces of P*t*BMA-Cl macroinitiator and P*t*BMA-*b*-C_{60} using RI detector and P*t*BMA-*b*-C_{60} using UV detector.

due to the similar characteristics of both polymers. However, we believe, the aggregation behavior in solution will not be significantly altered by this. A ^{13}C NMR spectrum was also obtained for the P*t*BMA-*b*-C_{60} polymer to confirm the formation of chemical bonding between P*t*BMA and C_{60}. However, there was no clear detectable peak at ~145 ppm, which is attributed to the resonance of the C_{60} moiety. This may be due to the low sensitivity of the carbon atoms of C_{60} caused by the loss of the 60-fold degeneracy of the original C_{60} molecules after being conjugated to the polymer chains. This also reinforces the covalent linkage between the C_{60} and P*t*BMA and not the physical trapping of C_{60} into the P*t*BMA matrix.[39]

The *tert*-butyl protecting groups of the well-defined P*t*BMA-*b*-C_{60} were removed by hydrolysis to obtain PMAA-*b*-C_{60}. The hydrolysis was confirmed by FT-IR (KBr pellet), which showed a broad peak at 3500 cm^{-1}, which is the characteristic absorption for carboxylic acid. In addition, the sharp peaks at 1393 and 1368 cm^{-1} correspond to the *tert*-butyl groups, which disappeared completely after hydrolysis, confirming that complete hydrolysis was achieved under acid conditions. This was further verified by end group analysis using potentiometric titration. The chemical formula of the copolymer can be expressed as $PMAA_{120}$-*b*-C_{60}. The amount of C_{60} incorporated into PMAA was further determined using TGA since C_{60} is thermally stable below 600 °C and PMAA decomposes at temperature below 500 °C. The weight percentage of the C_{60} calculated at 600 °C was ~5 wt %, which is consistent with the theoretical value of 4.5 wt %. The combination of GPC, FT-IR, and TGA results suggests the monoaddition between the PMAA and C_{60}.

Figure 2 shows comparison of the UV−vis spectra from PMAA-*b*-C_{60} in aqueous solution and C_{60} in cyclohexane. From the figure, it is evident that the PMAA-*b*-C_{60} in aqueous solution has three characteristic absorption peaks at 211, 258, and 334 nm, and these peaks are identical with the absorption peaks of C_{60} in cyclohexane. However, the relative absorption peak intensities are reduced, indicating the chemical modification of C_{60}.[39] The inset shows the absorption spectra in the visible wavelength region. The spectra are less structured, and no pronounced maxima were observed, which strongly supports the successful conjugation of PMAA chains onto C_{60}. This is also reinforced by the change in the color of the solution from purple (C_{60}) to yellow (PMAA-*b*-C_{60}). In addition, no obvious absorption

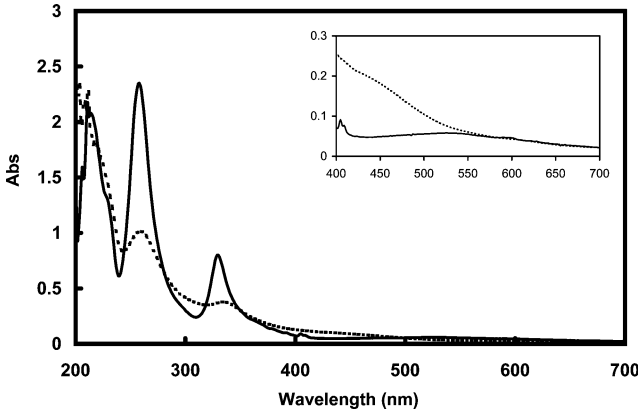

Figure 2. UV−vis spectra of C_{60} in cyclohexane (solid line) and PMAA-*b*-C_{60} in aqueous solutions at $\alpha = 1$ (dash line). The inset is the enlarged spectra in the visible region.

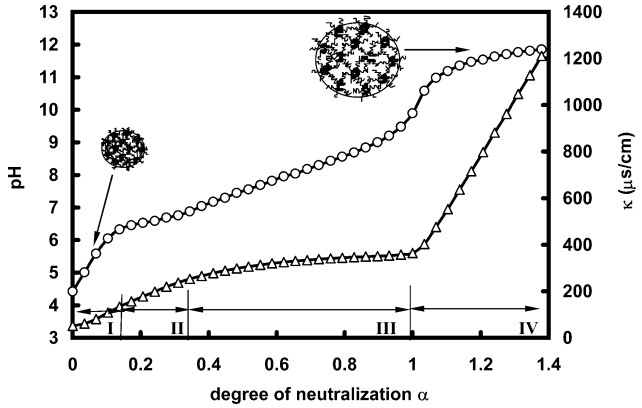

Figure 3. pH (open circle) and conductivity (open triangle) titration curves of 1 M NaOH into 0.2 wt % PMAA-*b*-C_{60} in aqueous solution at 298 K and 1 atm.

at 514 nm was observed, which indicates that the grafting of PMAA to C_{60} is a 1,2-addition and not a 1,4-addition.[35]

Potentiometric and Conductometric Titrations of PMAA-*b*-C_{60} Aqueous Solution. The degree of neutralization, α, of carboxylic groups can be defined

$$\alpha = \frac{[\mathrm{BASE}] + [\mathrm{H^+}] - [\mathrm{OH^-}]}{[\mathrm{COOH}]} \tag{1}$$

where [BASE], [H^+], and [OH^-] are the molar concentrations of added base, free hydrogen, and hydroxide ions, respectively, and [COOH] is the total concentration of methacrylic acid groups expressed in mol/L. Figure 3 shows the pH and conductivity curves plotted against the degree of neutralization (α) obtained from 1 M NaOH titrating into 0.2 wt % PMAA-*b*-C_{60} aqueous solution. The titration curves can be divided into four regions as marked in the figure. PMAA chains are in the acidic form at pH lower than 4.5. In region I, where α varies from 0 to 0.15, pH increases sharply with α, and this is attributed to the end neutralization of excess HCl from the synthesis process. With further increase of α to 0.35 in region II, the pH exhibits a gentler slope, which corresponds to the conformational change during the initial neutralization process. The details on the conformational change of PMAA during the neutralization has been reported by Mandel et al.[40] In region III, the slope of the potentiometric curve becomes steeper with increasing α until the neutralization process is completed at $\alpha = 1$. However, the decrease in the dependence of conductivity on α is evident in this region. This is attributed to counterion condensation which occurs when the distance between two charge groups is smaller than the Bjerrum length l_b as neutralization progresses. When α exceeds 1 (region IV), PMAA chains are fully neutralized at pH greater than 10.5, and only NaOH dilution is observed. From the potentiometric and conductometric titrations, useful information on the number-averaged M_n can be determined from end group analysis, in addition to the polymer conformation and counterion condensation during the neutralization process. A schematic diagram of the possible structures of PMAA-*b*-C_{60} aggregates at low and high pH is included in Figure 3.

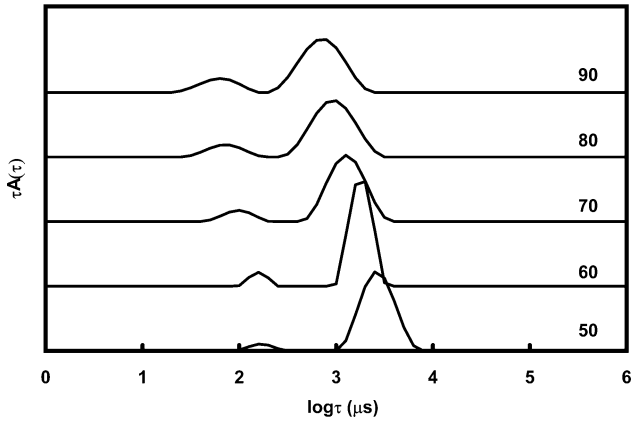

Figure 4. Angular dependence of the decay time distribution functions of 0.2 wt % PMAA-*b*-C_{60} in 0.5 M NaCl at $\alpha = 1$.

Laser Light Scattering of PMAA-*b*-C_{60} in Aqueous Solution. Laser light scattering was used to investigate the aggregation behavior of PMAA-*b*-C_{60} in aqueous solution. Figure 4 shows the decay time distribution functions of fully neutralized 0.2 wt % PMAA-*b*-C_{60} in 0.5 M NaCl aqueous solution at different scattering angles, where bimodal distribution is evident. With increasing scattering angle, both decay times decrease. The scattering vector q is defined as the difference in the wave vectors of scattering and incident lights with the value of

$$q = \frac{4\pi n \sin(\theta/2)}{\lambda} \tag{2}$$

where n is the refractive index of the solvent, θ is the scattering angle, and λ is the wavelength of the incident laser light in a vacuum. The dependence of decay rates Γ on scattering vector q was determined to examine the origin of both decay modes. Both Γ showed linear dependence on q^2, indicating that both decay modes are related to the translational diffusion of two types of scattering particles in solution, where the slope yields the translational diffusion coefficient, D.

The apparent hydrodynamic radius was then determined from the Stokes−Einstein equation:

$$R_{\mathrm{h,a}} = \frac{kT}{6\pi\eta D} = \frac{kTq^2}{6\pi\eta\Gamma} \tag{3}$$

where k is the Boltzmann constant, q is the scattering vector, η is the solvent viscosity, D is the translational diffusion coefficient at certain polymer concentration, and Γ is the decay rate. It was found that $R_{h,a}$ values of the fast and slow modes are 10 and 114 nm, respectively. Figure 5 shows the dependence of the apparent

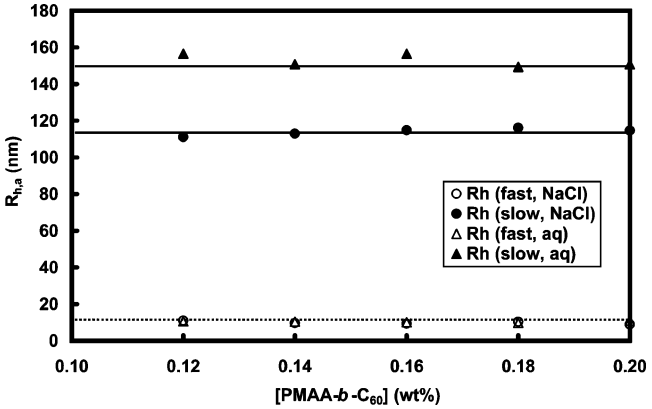

Figure 5. Dependence of $R_{h,a}$ on polymer concentration for PMAA-*b*-C_{60} in 0.5 M NaCl and aqueous solution at $\alpha = 1$.

Table 1. Laser Light Scattering Data of PMAA-*b*-C_{60} at Different pH Values and Salt Concentrations

[NaCl] (M)	α	R_h (fast) (nm)	R_h (slow) (nm)	M_w (10^6 g/mol)	R_g (nm)	R_g/R_h
0	0.0	6	91	37.9	210	2.31
0	0.2	6	117	39.7	262	2.24
0	0.4	6	135	41.9	312	2.31
0	0.8	9	147	39.6	334	2.27
0	1.0	10	153	40.4	335	2.19
0.2	1.0	10	118	10.8	261	2.21
0.5	1.0	10	114	8.5	208	1.82
1.0	1.0	10	105	7.5	168	1.60

hydrodynamic radius $R_{h,a}$ on polymer concentration in 0.5 M NaCl and aqueous solution at $\alpha = 1$. The hydrodynamic radii for both fast and slow modes in either 0.5 M NaCl or aqueous solution are independent of polymer concentration. Since the concentration dependence of the diffusion coefficient D can be described by

$$D = D_0(1 + k_D C + ...) \quad (4)$$

where D_0 is the diffusion coefficient at infinite dilute solution and k_D is the hydrodynamic virial coefficient. The independence of particle size on the polymer concentration indicates that k_D values for both particles are negligible within the experimental concentration range. By extrapolating $R_{h,a}$ to zero concentration, the hydrodynamic radius R_h was determined. The particle related to the fast decay mode in either 0.5 M NaCl or aqueous solution has an R_h of ~10 nm, which corresponds to the core−shell micelles in solution. On the other hand, the particle for the slow decay mode has an R_h of ~153 nm in aqueous solution and ~114 nm in 0.5 M NaCl solution, which should correspond to the large aggregates. It seems that an increase in salt concentration significantly reduces the size of large aggregate but not the micelle size. The calculated R_h values for both decay modes in different concentrations of salt solutions and α are summarized in Table 1.

Since particle sizes in either aqueous or salt solution are independent of polymer concentration, static light scattering was carried out to determine the weight-averaged molecular weight M_w and the z-averaged radius of gyration R_g.

$$\left(\frac{KC}{R_\theta}\right)^{0.5} = \left(\frac{1}{M_w}\right)^{0.5}\left(1 + \frac{1}{6}q^2 R_g^{\,2}\right)(1 + A_2 M_w C) \quad (5)$$

where K ($=4\pi^2 n^2 (dn/dC)^2/N_A\lambda^4$) is an optical constant with N_A, n, and λ being the Avogadro number, the solvent refractive index, and the wavelength of the light in a vacuum, respectively. C is the polymer concentration in g/mL, and R_θ is the excess Rayleigh ratio at scattering angle θ. The refractive index increment of polymer solution (dn/dC) was measured using a Brookhaven BI-DNDC differential refractometer. The z-averaged radius of gyration R_g, the second virial coefficient A_2, and the weight-average molecular weight M_w were determined from the above equation by extrapolating to zero concentration and zero angle as shown by the Berry plot in Figure 6. The calculated apparent M_w and R_g values are shown in Table 1.

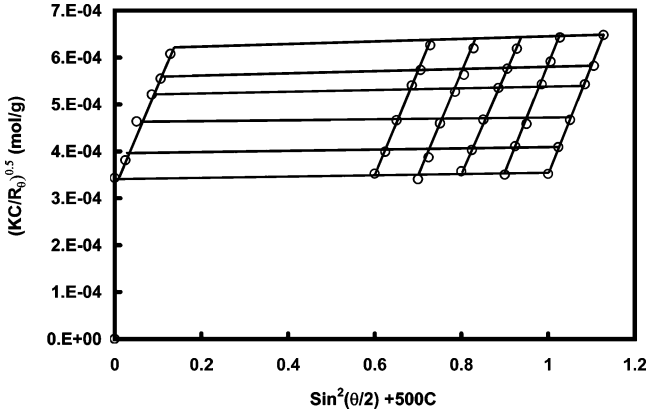

Figure 6. Typical Berry plot of PMAA-*b*-C_{60} at $\alpha = 1$ in 0.5 M NaCl aqueous solution.

Because of the large R_g values of aggregates in solution, the translational decay modes may include internal modes for $qR_g \gg 1$. To further elucidate the characteristics of the aggregate, cumulant was used to analyze the time correlation functions. For polydispersed decay time distribution, the first cumulant gives the effective decay rate Γ_e and second cumulant is related to the overall polydispersity.[41] At $qR_g > 1$, the relationship between Γ_e and qR_g can be expressed by

$$\frac{\Gamma_e}{q^2} = D_0(1 + K(qR_g)^2) \quad (6)$$

where the coefficient K is dependent on the structure and the draining behavior of scattering objects in solution.[42] The relationship between $\Gamma_e/(q^2 k_B/\eta)$ and qR_g was first examined. For fully neutralized PMAA-*b*-C_{60} in salt-free solution, it was found that $\Gamma_e/(q^2 k_B/\eta)$ increases with qR_g at $qR_g > 1.5$. This may be due to the dependence of $A_s/(A_f + A_s)$ (A_f and A_s are the amplitude of the fast and slow modes respectively) on the measurement angle based on previous ILT analysis, or it may also be attributed to the internal motion of the core−shell micelles or PMAA chains. The relationship between $\Gamma_e/(q^3 k_B/\eta)$ and qR_g was further examined to study the internal motion. It was found that the value of $\Gamma_e/(q^3 k_B/\eta)$ decreases with increasing qR_g and reaches an asymptotic value at $qR_g > 1.5$, which corresponds to the Rouse−Zimm relaxation inside the aggregates. This internal motion may have been contributed by the stiff polyelectrolyte backbone; however, this contribution is too small to be accurately determined.

At $\alpha = 1$, all PMAA segments are fully neutralized, and they possess polyelectrolyte characters. Thus, addition of salt can influence the polyelectrolyte properties in solution as well as the association behavior of the polyelectrolyte containing amphiphiles. LLS experiments were conducted to examine the effect of

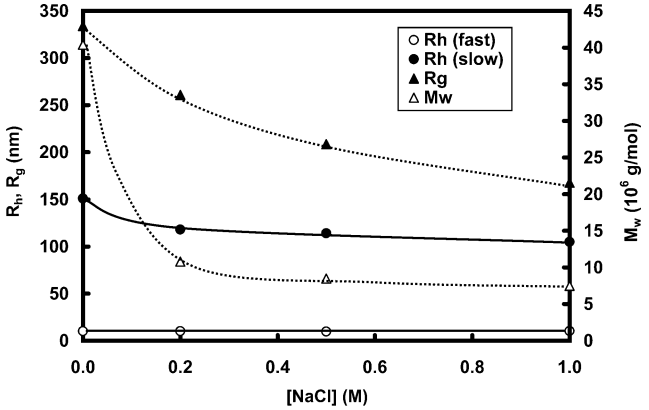

Figure 7. Effect of salt concentration on R_h for 0.2 wt % PMAA-*b*-C_{60} at $\alpha = 1$.

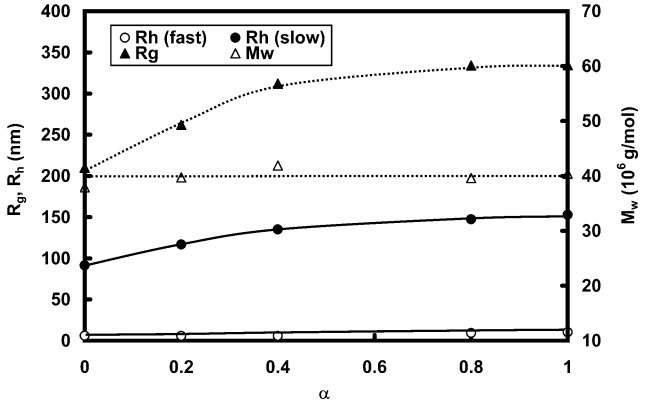

Figure 8. Dependence of R_h on degree of neutralization α for 0.2 wt % PMAA-*b*-C_{60} in aqueous solution.

salt concentration on the aggregation behavior of PMAA-*b*-C_{60} at fully neutralized condition. Figure 7 shows the dependence of the hydrodynamic radii (R_h) of PMAA-*b*-C_{60} micelles and aggregates on NaCl concentration at fully neutralized condition. The R_h of fast mode remains unchanged with increasing salt concentration and possess an averaged value of 10 nm. On the other hand, the R_h of the slow mode decreases sharply at low salt concentrations and marginally decreases at high salt concentrations, where R_h of the large aggregate decreases gradually from ~153 nm in aqueous solution to ~105 nm with the addition of 1 M NaCl. The formation of PMAA-*b*-C_{60} micelles and aggregates is controlled by the balance between hydrophobic attraction and electrostatic repulsion. Addition of NaCl shields the electrostatic interaction between charged polyelectrolyte segments, enhancing the chain flexibility of the PMAA segments. At the same time, addition of salt also increases solvent polarity. The increase in the aggregation number and the decrease in the hydrodynamic size of fully neutralized PMAA segments maintain a constant micellar size with increasing NaCl concentration. The large aggregates are composed of many individual micelles, where these micelles are stabilized by the electrostatic interactions from the charged polyelectrolyte backbones and counterions. With increasing salt concentration, the carboxylate groups are shielded by oppositely charged counterions, and the PMAA chains shrink, causing a reduction in the particle size of the aggregate.

SLS was performed to examine the effect of salt concentration on the weight-averaged molecular weight M_w and R_g as shown in Figure 7. Both M_w and R_g decrease with the addition of NaCl. Since there are two types of particles in solution, M_w and R_g are more sensitive to the large particle. A sharp decrease in M_w and R_g is evident at [NaCl] < 0.2 M, which suggests that smaller aggregates are produced. At [NaCl] > 0.2 M, the shrinkage of neutralized PMAA segments dominates as evident by the negligible change in M_w and a continuous reduction in R_g. This trend can also be observed from the R_g/R_h value as shown in Table 1, where the R_g/R_h value remains constant at 2.2 at [NaCl] < 0.2 M and decreases to 1.6 at [NaCl] of 1.0 M. The values of R_g/R_h can be used to evaluate the possible morphology of scattering objects in solution. Both theoretical and experimental studies indicate that monodispersed hard spheres possess a R_g/R_h value of 0.774. However, our measured R_g/R_h values are much higher, and we believe that this may be caused by the porosity of the spherical particles. In salt-free or low salt solution, the fully neutralized PMAA chains behave as polyelectrolytes, and with increasing salt concentration, the electrostatic repulsion is shielded and the chain stiffness decreases. As a result, the decrease of R_g/R_h with the addition of excess amount salt is observed. Laser light scattering experiments suggest that addition of salt has an impact on aggregation behavior of PMAA-*b*-C_{60}.

The effect of α on the aggregation behavior of PMAA-*b*-C_{60} was also examined. Figure 8 shows the hydrodynamic radius of both particles at different α values. The R_h of the fast mode increases from 6 to 10 nm when α changes from 0 to 0.4 and then remains rather constant throughout the rest of neutralization process. R_h of the large aggregate increases from ~90 ($\alpha = 0$) to ~152 nm ($\alpha = 1$). The fast mode corresponds to core−shell micelle comprising of hydrophobic fullerene core that is stabilized by hydrophilic PMAA corona. With the neutralization of PMAA segments, the coiled chains become expanded and increase in size. Since the large aggregate corresponds to the secondary association of individual micelles (commonly referred to as large compound micelle, LCM), addition of NaOH neutralizes and ionizes the carboxylic groups on the shell layer, which increases the electrostatic potential on the micellar surface. The shell layer may expand to a certain extent, driven by the electrostatic repulsion between these charged carboxylate groups, which also increases the chain rigidity. Therefore, the increase in the particle size is attributed to the neutralization and swelling of the hydrophilic PMAA segments. SLS was also conducted, and the data are summarized in Table 1 and Figure 8. It is evident that R_g show similar trends as R_h, while M_w and R_g/R_h remain constant, which indicates that the swelling of PMAA chains rather than the structural reorganization is the dominant process.

Transmission Electron Microscopy. Transmission electron microscopy (TEM) was used to investigate the morphology of large PMAA-*b*-C_{60} aggregates in solution. Figure 9 compares the morphology of PMAA-*b*-C_{60} aggregates at different pH values. It is evident that the abundance of spherical aggregates at either low or high pH values. These aggregates are believed to be large compound micelles (LCM), as closer examination on a single aggregate revealed smaller individual spherical micellar aggregates within a single large aggregate. The radii of the LCM at pH 4 and pH 12 ranges from 85 to 120 nm and 125 to 165 nm, respectively, and the results from TEM are consistent with DLS results.

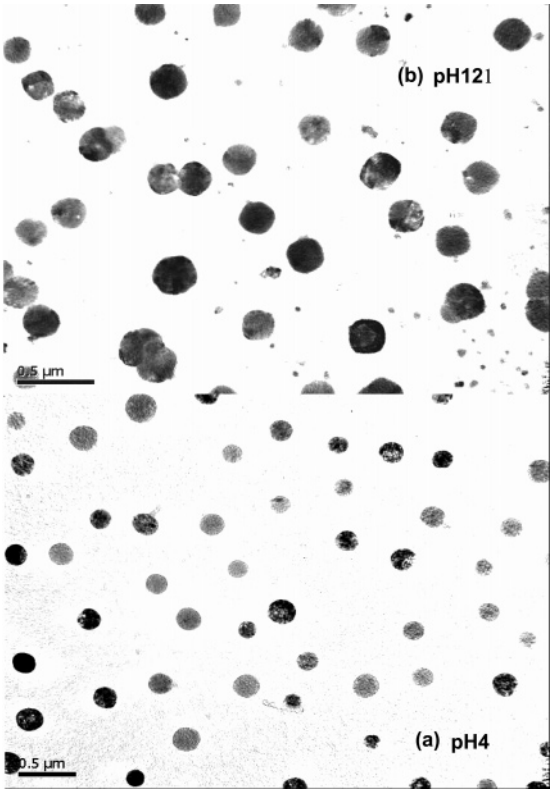

Figure 9. Transmission electron micrographs of PMAA-*b*-C_{60} at different pH values (a) pH 4 and (b) pH 12.

Conclusions

A well-defined water-soluble pH-responsive PMAA end-capped C_{60} was synthesized using ATRP technique. The aggregation behaviors of PMAA-*b*-C_{60} block copolymer in aqueous solution were investigated using potentiometric and conductometric titrations, DLS, SLS, and TEM by varying polymer concentration, degree of neutralization, and salt concentration. In aqueous solution, micelles and secondary aggregates consisting of large compound micelles (LCM) are present in solution. Their hydrodynamic sizes are found to be independent of polymer concentration. The core−shell micelle possesses a R_h of 10 nm, which is independent of salt concentration, while the R_h of LCM decreases with the addition of NaCl. R_h of the LCM and the micelles increase with increasing the degree of neutralization α, which is attributed to the swelling the PMAA segments.

Acknowledgment. The authors acknowledge the financial support provided by the Singapore-MIT Alliance (SMA) and Nanyang Technological University, Singapore.

References and Notes

(1) Sauer, M.; Meier, W. *Chem. Commun.* **2001**, *1*, 55.
(2) Zhang, X.; Matyjaszewski, K. *Macromolecules* **1999**, *32*, 1763.
(3) Eisenberg, A.; Rinaudo, M. *Polym. Bull. (Berlin)* **1990**, *24*, 671.
(4) Schuch, H.; Klingler, J.; Rossmanith, P.; Frechen, T.; Gerst, M.; Feldthusen, J.; Müller, A. H. E. *Macromolecules* **2000**, *33*, 1734.
(5) Stepanec, M.; Podhajecka, K.; Tesarova, E.; Prochazka, K.; Tuzar, Z.; Brown, W. *Langmuir* **2001**, *17*, 4240.
(6) Riegel, I. C.; Eisenberg, A. *Langmuir* **2002**, *18*, 3358.
(7) Shen, H.; Eisenberg, A. *J. Phys. Chem. B* **1999**, *103*, 9473.
(8) Zhang, L.; Eisenberg, A. *J. Am. Chem. Soc.* **1996**, *118*, 3168.
(9) Cheng, G.; Böker, A.; Zhang, M.; Krausch, G.; Müller, A. H. E. *Macromolecules* **2001**, *34*, 6883.
(10) Förster, S.; Hermsdorf, N.; Leube, W.; Schnablegger, H.; Regenbrecht, M.; Akari, S.; Lindner, P.; Böttcher, C. *J. Phys. Chem. B* **1999**, *103*, 6657.
(11) Gohy, J. F.; Willet, N.; Varshney, S.; Zhang, J. X.; Jerome, R. *Angew. Chem., Int. Ed.* **2001**, *40*, 3214.
(12) Talingting, M. R.; Munk, P.; Webber, S. E.; Tuzar, Z. *Macromolecules* **1999**, *32*, 1593.
(13) Terreau, O.; Bartels, C.; Eisenberg, A. *Langmuir* **2004**, *20*, 637.
(14) Curl, R. F.; Smalley, R. E. *Science* **1988**, *242*, 1017.
(15) Kroto, H. *Science* **1988**, *242*, 1139.
(16) Jeng, U.; Lin, T. L.; Hu, Y.; Chang, T. S.; Canteenwala, T.; Chiang, L. Y.; Frielinghaus, H. *J. Phys. Chem. A* **2002**, *106*, 12206.
(17) Konarev, D. V.; Lyubovskaya, R. N.; Drichko, N. V.; Yudanova, E. I.; Shulga, Y. M.; Litvinov, A. L.; Semkin, V. N.; Tarasov, B. P. *J. Mater. Chem.* **2000**, *10*, 803.
(18) Song, T.; Dai, S.; Tam, K. C.; Lee, S. Y.; Goh, S. H. *Langmuir* **2003**, *19*, 4798.
(19) Zhou, S.; Burger, C.; Chu, B.; Sawamura, M.; Nagahama, N.; Toganoh, M.; Hackler, U. E.; Lsobe, H.; Nakamura, E. *Science* **2001**, *291*, 1944.
(20) Tokuyarna, H.; Yamago, S.; Nakamura, E.; Shiraki, T.; Sugiura, Y. *J. Am. Chem. Soc.* **1993**, *115*, 7918.
(21) Sitharaman, B.; Asokan, S.; Rusakova, I.; Wong, M. S.; Wilson, L. J. *Nano Lett.* **2004**, *4*, 1759.
(22) Takenaka, S.; Yamashita, K.; Takagi, M.; Hatta, T.; Tanaka, A.; Tsuge, O. *Chem. Lett.* **1999**, *4*, 319.
(23) Cassell, A. M.; Scrivens, W. A.; Tour, J. M. *Angew. Chem., Int. Ed.* **1998**, *37*, 1528.
(24) Zhou, S.; Burger, C.; Chu, B.; Sawamura, M.; Nagahama, N.; Toganoh, M.; Hackler, U. E.; Lsobe, H.; Nakamura, E. *Science* **2001**, *291*, 1944.
(25) Chiang, L. Y.; Bhonsle, J. B.; Wang, L.; Shu, S. F.; Chang, T. M.; Hwu, J. R. *Tetrahedron* **1996**, *52*, 4963.
(26) Okamura, H.; Miyazono, K.; Minoda, M.; Miyamoto, T. *Macromol. Rapid Commun.* **1999**, *20*, 41.
(27) Friedman, S. H.; Decamp, D. L.; Sijbesma, R. P.; Srdanov, G.; Wudl, F.; Kenyon, G. L. *J. Am. Chem. Soc.* **1993**, *115*, 6506.
(28) Song, T.; Goh, S. H.; Lee, S. Y. *Macromolecules* **2002**, *35*, 4133.
(29) Tan, C. H.; Ravi, P.; Dai, S.; Tam, K. C.; Gan, L. H. *Langmuir* **2004**, *20*, 9882.
(30) Yang, J.; Li, L.; Wang, C. *Macromolecules* **2003**, *36*, 6060.
(31) Song, T.; Dai, S.; Tam, K. C.; Lee, S. Y.; Goh, S. H. *Polymer* **2003**, *44*, 2529.
(32) Okamura, H.; Ide, N.; Minoda, M.; Fukuda, T.; Komatsu, K. *Macromolecules* **1998**, *31*, 1859.
(33) Wang, X.; Goh, S. H.; Lee, S. Y.; Wu, C. *Macromolecules* **1999**, *32*, 2786.
(34) Ford, W. T.; Lary, A. L.; Mourey, T. H. *Macromolecules* **2001**, *34*, 5819.
(35) Zhou, P.; Chen, G. Q.; Hong, H.; Du, F. S.; Li, Z. C.; Li, F. M. *Macromolecules* **2000**, *33*, 1948.
(36) Yang, D.; Li, L.; Wang, C. *Mater. Chem. Phys.* **2004**, *87*, 114.
(37) Dai, S.; Ravi, P.; Tan, C. H.; Tam, K. C. *Langmuir* **2004**, *20*, 8569.
(38) Gan, L. H.; Ravi, R.; Mao, B. W.; Tam, K. C. *J. Polym. Sci., Part A: Polym. Chem.* **2003**, *41*, 2688.
(39) Tang, B. Z.; Xu, H.; Lam, J. W. Y.; Lee, P. P. S.; Xu, K.; Sun, Q.; Cheuk, K. K. L. *Chem. Mater.* **2000**, *12*, 1446.
(40) Mandel, M.; Leyte, J. C.; Stadhouder, M. G. *J. Phys. Chem.* **1967**, *71*, 603.
(41) Brown, W. *Dynamic Light Scattering*; Clarendon Press: Oxford, 1993.
(42) Burchard, W.; Schmidt, M.; Stockmayer, W. H. *Macromolecules* **1980**, *13*, 580.

MA0480547